

PAPER • OPEN ACCESS

Influence of the conductive coating on combined CPEM and Raman analysis.

To cite this article: F Mura *et al* 2023 *J. Phys.: Conf. Ser.* **2579** 012012

View the [article online](#) for updates and enhancements.

You may also like

- [The 2018 correlative microscopy techniques roadmap](#)
Toshio Ando, Satya Prathyusha Bhamidimarri, Niklas Brending et al.
- [STORM without enzymatic oxygen scavenging for correlative atomic force and fluorescence superresolution microscopy](#)
Liisa M Hirvonen and Susan Cox
- [Optimising correlative super resolution and atomic force microscopies for investigating the cellular cytoskeleton](#)
Riley B Hargreaves, Ashley M Rozario, Thomas M McCoy et al.



The Electrochemical Society
Advancing solid state & electrochemical science & technology

247th ECS Meeting
Montréal, Canada
May 18-22, 2025
Palais des Congrès de Montréal

Showcase your science!

Abstract submission deadline extended: December 20

ECS UNITED

The poster features a large graphic of a hand holding a globe with three vertical bars, set against a background of a grid of dots and wavy lines. The ECS logo is in the top left, and the meeting details are in the top right. A green circle in the bottom right contains the text about the extended abstract submission deadline.

Influence of the conductive coating on combined CPEM and Raman analysis.

F Mura¹, S Dinarelli², C Mancini¹, A Proietti¹, L Buccini¹, S Silvestri¹, D Passeri¹, M Rossi¹

¹ Department of Basic and Applied Sciences for Engineering, Sapienza University Of Rome, Rome (Italy).

² Institute of the Structure of Matter, National Research Council (CNR), Rome, Italy.

francesco.mura@uniroma1.it

Abstract. The sample preparation is one of the fundamental steps to obtain a successful correlative microscopy experiment, and for non-conductive materials the deposition of a thin metal coating is often mandatory for a good SEM observation. Nevertheless, in case of correlative experiment, where AFM and Raman spectroscopy are involved in the workflow, this deposition will have a direct influence on both the analysis. In this paper, an investigation about the most common conductive materials used in SEM sample preparation, such as chromium, graphite and gold, and their behaviour in the construction of correlative microscopy workflow is proposed, showing in our results, that chromium is the best choice for this type of combined analysis.

1. Introduction

During the last two decades, the rapid and continuous development of technology, especially in computer science, has led to a constant improvement for numerous microscopy and spectroscopy techniques, increasing not only their spatial resolution, but making them more interconnected. For this reason, one of the most important future challenges, not only concerning the researchers, but above all the instrument manufacturers, will regard the treatment and organization of all the experiment data, where the characterization of a specimen will be given from the contributions of several instruments and analysis techniques. For this reason, giving an unambiguous and defined context to this enormous flow of data will be one of the most difficult tasks for a researcher. In this scenario, year after year, the so-called correlative microscopy and the development of new workflows for rapid and efficient analysis has become a central topic in the field of microscopies [1]. Although the CLEM, acronym for Correlative Light to Electron Microscopy, has been the first to be developed in the 60s [2,3], still retains a central role for its immediate impact on the medical and life sciences [1]. Nevertheless, over the last years, new combinations of different microscopy and spectroscopy techniques started to emerge, including instruments like Atomic Force Microscopy (AFM) or Raman spectroscopy [4, 5], bringing many companies to develop a series of new tools that combine them together, like the RISE system, born from the partnership between Zeiss and WITec [6], with the aim to construct an integrated Raman and Scanning Electron Microscopy (SEM) instrument, or the Litescope AFM-in-



SEM from Nenovision [7, 8], capable to perform several AFM techniques inside the chamber of an electron microscope. These new devices allow not only to perform a combined analysis without transferring the sample from an instrument to another, resulting not only in a enormous time saving, but above all in a more precise and controlled workflow. However, as highlighted by the large number of protocols developed for the CLEM [9], a good sample preparation is a very important step in the construction of a valid workflow: the sample must preserve its integrity and, at the same time, avoid any type of artefact or false signal in the electron and optical microscopy. In this context, a correlative experiment, made of Raman spectroscopy and CPEM (Correlative Probe to Electron Microscopy) is performed with an innovative and integrated AFM-in-SEM system, the Litescope® by Nenovision [10]. And an investigation the influence of gold, chromium and graphite, as conductive layer, normally deposited by sputtering [11] is evaluated.

2. Materials & methods

2.1. Sample preparation

A (111) silicon wafer from Siliconix has been cut with a diamond scribe in small pieces of approx. $1.5\text{ cm} \times 1.5\text{ cm}$, cleaned with isopropyl alcohol and dried under a gentle flux of air. Next, a conductive coating has been deposited on their surface using a Quorum Q150T sputter machine, producing a series of samples sputtered with three target materials, gold, chromium, and graphite, having an increasing thickness of 10, 25 and 50 nm. Gold and chromium thin films are grown through the magnetron sputter coating process, while the carbon films are deposited from high vacuum evaporation of carbon rods, the so-called Brandley method [11].

2.2. AFM-in-SEM

The AFM images were acquired directly inside the SEM chamber of VEGA electron microscope (from TESCAN), in high vacuum conditions, by a particular model of AFM, the Litescope (from Nenovision), directly allocated on the sample holder of the electron microscope. The area of interest, $6 \times 6\ \mu\text{m}^2$ area without visible imperfections, is localised by the SEM, and then scanned by the AFM tip. The measurements were performed in tapping mode with Akiyama tips that are self-sensing and self-actuating, with nominal elastic constant and frequency of 5 N/m and 45 kHz, respectively [8]. The AFM analysis of the surface root mean square roughness (Rq) was performed using Gwyddion software [12], by picking a $4 \times 4\ \mu\text{m}^2$ area in five regions of the sample.

2.3. Micro-Raman

Raman spectra were collected at room temperature using the InVia™ confocal Raman Spectrometer (from Renishaw), with 250 mm focal length. The analysis has been conducted using three excitation lines: one in the NUV range (354.8 nm), the Zouk™ from the Cobolt 05-01 series, the green line at 532.1 nm, generated by the Nd:YAG continuous-wave diode-pumped solid state laser (from Renishaw), and the red line at 632.8 nm, obtained from an HeNe laser (from Renishaw). Light has been focused on the sample through two short WD objectives: a 40× with NA = 0.47 for the NUV laser (from ThorLabs) and a N PLAN EPI 100× with NA = 0.85 (from Leica Microsystems) for the visible lines. The spectrum calibration has been performed before each measurement through the internal reference of both silicon and the Ne-Ar light available in the spectrometer. All the spectra have been acquired in the $120\text{-}3200\text{ cm}^{-1}$ spectral range with an exposition time of 10 s and 2 accumulations. The laser power was set as following: 3 mW - NUV line; 2.5 mW - green line; 2 mW - red line. For each sample a punctual measure has been acquired. The software WiRE™ 4.4 and SpectraGryph have been used for the spectra processing. Normalized intensities of each band were calculated considering the ratio between their height and the intensity of the most prominent peak in the spectrum.

3. Results and discussion

3.1. CPEM analysis

The SEM observation in fig. 1 shows minor qualitative differences in morphology among the samples covered with the maximum amounts of coating, although some roughness can be observed from the sample covered with gold. This is mainly due to a better response of the material to the electron beam due to its high atomic number and to the formation of larger grains during the sputter process. However, the graphite coating resulted to have many irregularities, especially for the 25 nm sample, with the presence of aggregates of dimension larger than 300 nm, but this is a well-known issue for high vacuum evaporation methods, like the Brentley method [13]. For this reason, to perform a precise and controlled AFM scanning, areas without big defects have been selected.

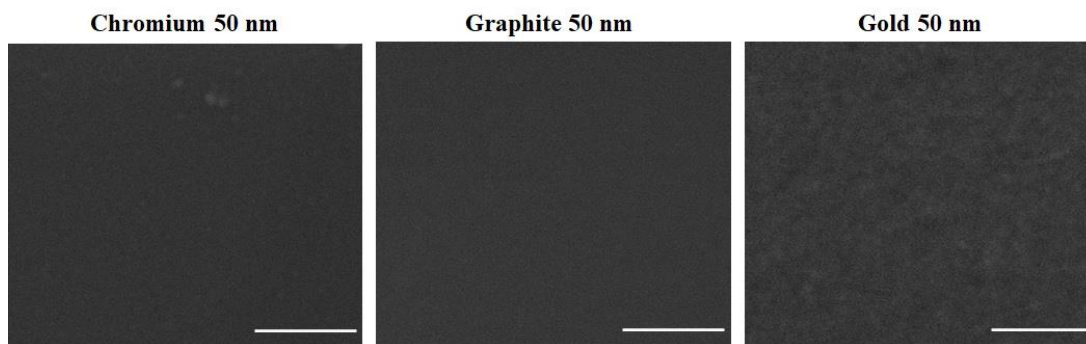


Figure. 1: SEM images performed on the three different coatings with thickness layer of 50 nm (scale bar 500 nm).

The AFM image on the native silicon sample, as shown in fig. 2-A, has a morphology typical of an oxidised surface of Si, with a randomly structured layer of oxide of few nanometers in height and some round shaped contaminants of few tens of nanometers in diameter. The intrinsic surface roughness of the silicon was found to be 1.54 ± 0.21 nm.

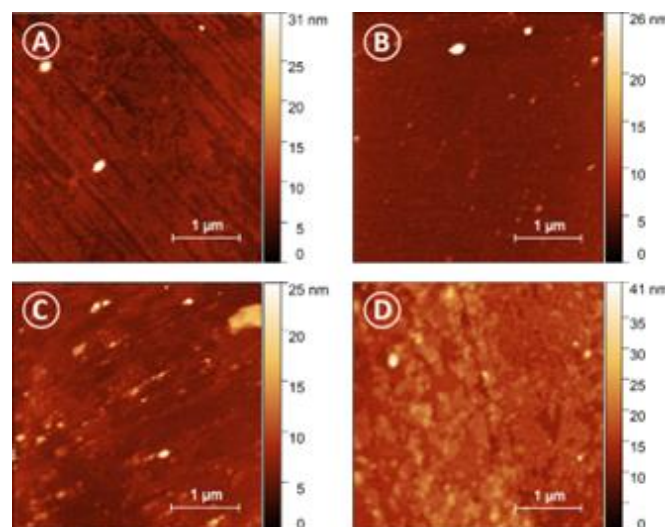


Figure. 2: Typical AFM images performed onto pristine silicon (panel A), silicon covered with 10nm of chromium (panel B), 25nm of gold (panel C) and 50nm of graphite (panel D).

The choice of adopting an oxidised silicon, without making a previous cleaning of the surface, is due firstly for mimicking the presence of nano-sized structures randomly distributed all over the sample, and secondly to have a better evaluation of the effects created by the different thickness and coating materials. As reported in the tab. 1, the measured roughness does not change for different amounts of chromium and gold, meaning that the general topography of the sample is not altered. The same results have been found also for the graphite coating, except for the specimen with the 25 nm thickness, where, as reported previously, quasi-spherical structures with diameter of several microns have been found.

Table 1. Average roughness measured in nanometers for the chromium, graphite, and gold coating at different thickness (10, 25 and 50 nm) and for the pristine silicon.

	10 nm	25 nm	50 nm
Chromium	1.35±0.04	1.61±0.14	1.74±0.04
Graphite	1.75±0.15	9.15±0.36	2.35±0.20
Gold	1.75±0.09	1.49±0.12	1.36±0.07
Pristine Silicon	1.54±0.21		

It should be noted, at first, a very peculiar aspect: the standard deviation value of 0.21 nm obtained for the pristine Silicon was the bigger among all the other samples, a clear indication that performing a coverage of the specimen grants more homogeneous surfaces.

Histograms with the measured Rq for the three coating materials are reported in fig. 2.

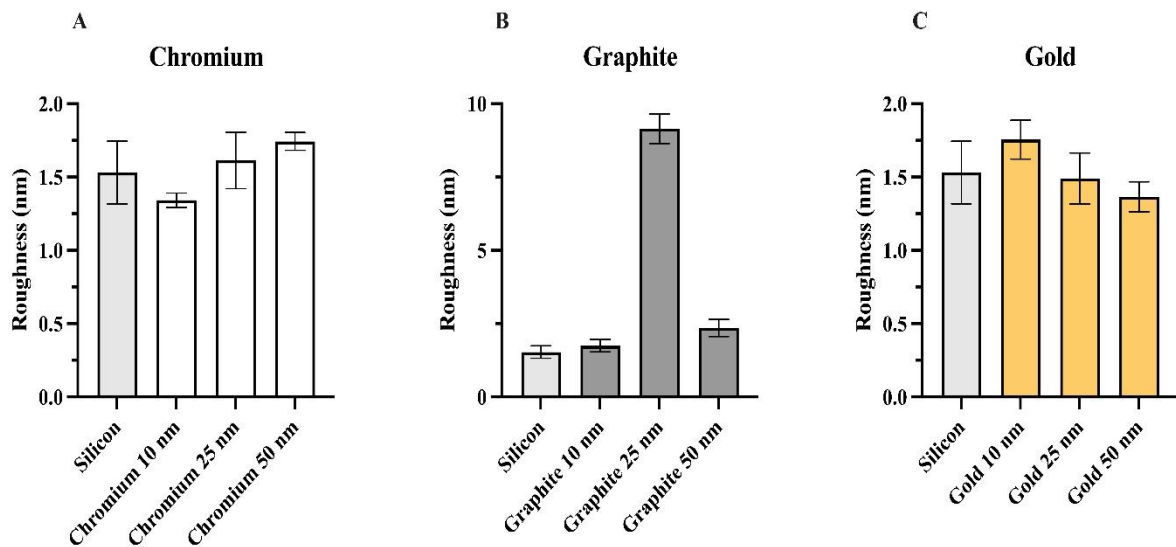


Figure 3. Average roughness and relative error for the chromium (panel A), graphite (panel B) and gold coating at different thickness.

Looking the fig. 3-A, from the covering of the surface with growing amount of chromium it's possible to point out two important aspects: a) as expected, the roughness progressively increases, raising from

$1,35 \pm 0,04$ nm up to $1,74 \pm 0,04$ nm; b) the thicker the coating, the more homogeneous the coverage of the sample results, since the standard deviation drops down to very low values. However, it is also worth noticing that all the measured values were still compatible with the R_q value of the pristine silicon, giving further confirmation that chromium is one of the best options to create a conductive coating for high-resolution imaging [10]. On the other hand, looking at fig. 2-B, the R_q measurements for the graphite coating exhibit values that are significantly higher the standard of the pristine Silicon, especially for the 50 nm case, meaning that the original morphology of the sample has undergone important changes. Lastly, the increase of the thickness of the gold coating results in a reverse trend in the surface roughness, although these data remain consistent with the ones of the uncoated sample (fig. 2-C). This opposite trend between gold and chromium can be correlated with the intrinsic nature of these two metals, since chromium progressively grows on what was already deposited without generating further interactions, while gold tends to coalesce with the previous deposition, generating thicker grains, thus leading to smoother surfaces [10].

3.2 Micro-Raman analysis

To perform a correct correlative microscopy that includes SEM, AFM and Raman, it's important to understand if (and how much) the presence and quantity of a conductive coating material can generate false peaks or artefacts on the final spectrum of the silicon (111) substrate. Fig. 4 shows the acquisitions obtained with increasing thickness of chromium: here the effects of the chrome coating resulted in a gradual rise of the noise in the acquired spectra. Moreover, this variation is inversely proportional to the laser wavelength, with an exponential trend when the N-UV laser is used.

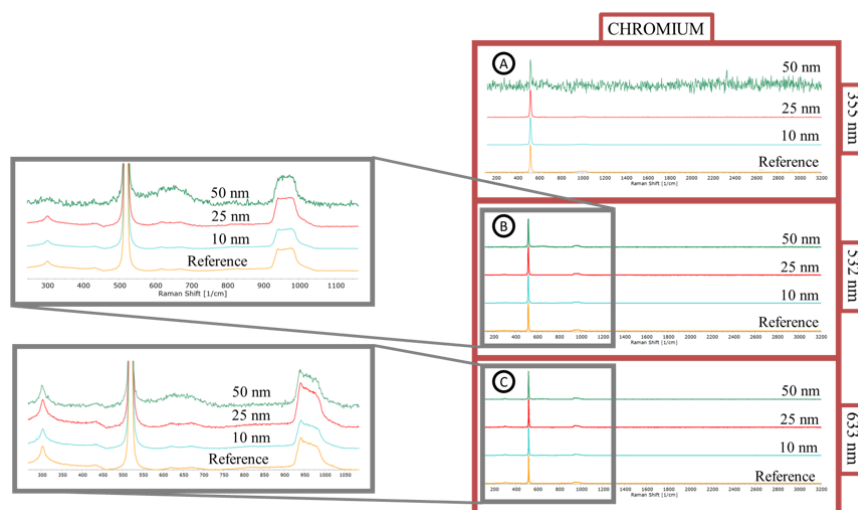


Figure 4. Raman spectra for the (111) silicon sample coated with a chromium layer of 10, 25 and 50 nm thickness, in navy blue, red and green lines respectively, measured using N-UV (panel A), green (panel B) and red (panel C) laser.

A similar behaviour resulted for the graphite coating, even if in this case the impact was smaller due to the non-uniform deposition of the film (fig. 5). In this case a visible peak related to the graphite appears at the 1600 cm^{-1} , mostly using the N-UV laser case because of its smaller penetration depth.

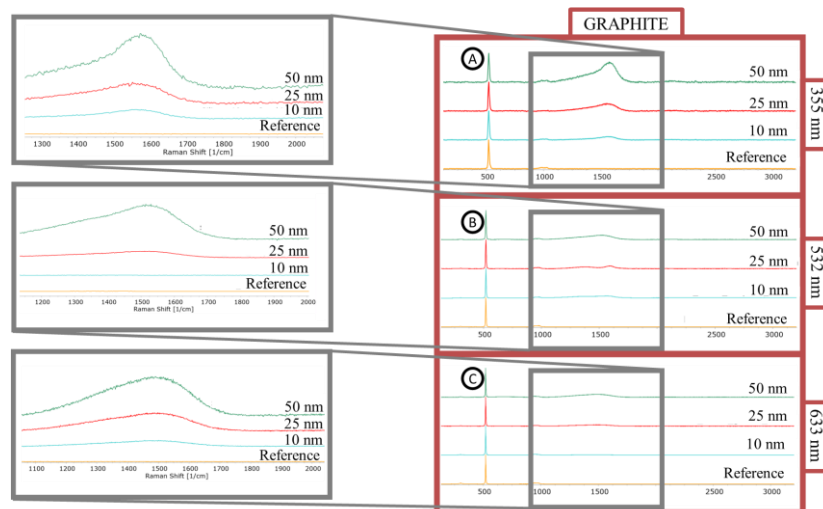


Figure 5. Raman spectra for the (111) silicon sample coated with a graphite layer of 10, 25 and 50 nm thickness, in navy blue, red and green lines respectively, measured using N-UV (panel A), green (panel B) and red (panel C) laser.

Looking at the spectra acquired having a gold coating (fig. 6), it's quite evident how this material is not suitable for a correlative microscopy that includes a Raman analysis. In fact, the background noise is so intense that it's difficult or even impossible to identify the substrate peak, particularly when using low penetration depth excitation lines such as the N-UV laser. The thicker coating of 50 nm represents a problem, even for the green excitation line, for the low intensity of the main silicon peak in the acquired spectrum that makes its identification problematic.

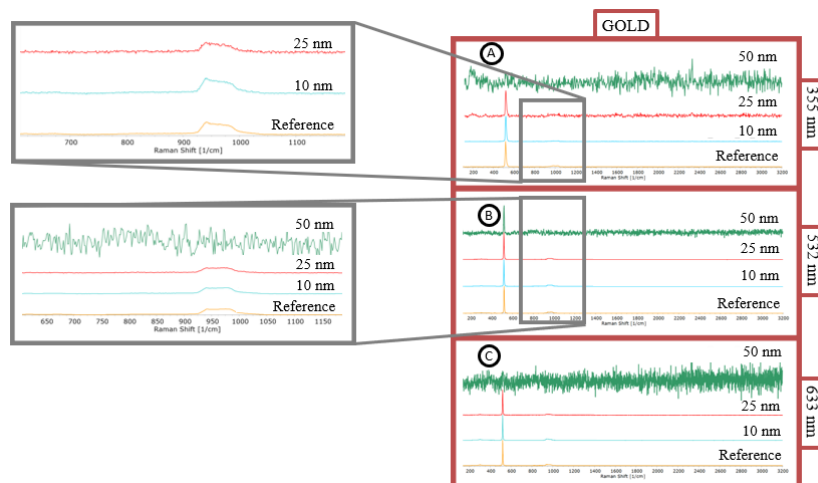


Figure 6. Raman spectra for the (111) silicon sample coated with a gold layer of 10, 25 and 50 nm thickness, in navy blue, red and green lines respectively, measured using N-UV (panel A), green (panel B) and red (panel C) laser.

4. Conclusion

In the creation of a new workflow that implies a correlative microscopy based on CPEM and Raman spectroscopy, our study demonstrated that the presence of a very thin metal conductive layer on a sample does not introduce significant alterations in the actual morphology of a sample during an AFM

measurement. Conversely, the choice of the coating metal and its thickness has a direct and occasionally dramatic influence on the Raman analysis. The deposited coating produces indeed a decrease in the signal intensity, which in some cases can even lead to the complete covering of significant peaks related to the sample, as observed in the case of the 50 nm gold coating. The choice of a graphite coating is also highly unrecommended: it introduces not only the presence of large particles on the sample surface, but also a broad and prominent peak in the Raman acquisition that can compromise the characterization of carbon-based specimens. In conclusion, chromium can be considered as the best choice, even at high thicknesses: it leaves unchanged the original morphology of the sample, and, most importantly, does not add any false peaks to the Raman spectra.

Acknowledgments

This research has been realized with the financial support of the projects CHALLENGES - Real time nano CHAracterization reLatEd techNoloGiES, granted by European Commission (call H2020-NMBP-TO-IND-2019) and ATOM - Advanced Tomography and Microscopies, granted by Lazio Region (call "Open infrastructures for research").

References

- [1] Ando T, Bhamidimarri SP, Brending N, Colin-York H, Collinson L, De Jonge N, de Pablo PJ, Debroye E, Eggeling C, Franck C, Fritzsche M, Gerritsen H, Giepmans BNG, Grunewald K, Hofkens J, Hoogenboom JP, Janssen KPF, Kaufmann R, Klumperman J, Kurniawan N, Kusch J, Liv N, Parekh V, Peckys DB, Rehfeldt F, Reutens DC, Roeffaers MJB, Salditt T, Schaap IAT, Schwarz US, Verkade P, Vogel MW, Wagner R, Winterhalter M, Yuan H and Zifarelli G, 2018 *J. Phys. D: Appl. Phys.* **51** 443001
- [2] Morgan C, Godman GC, Breitenfeld PM and Rose HM, 1960 *J. Exp. Med.* **112** 373–382
- [3] Morgan C, Godman GC, Breitenfeld PM and Rose HM, 1960 *J. Exp. Med.* **112** 383–402
- [4] Schmidt R, Nachtnebel M, Dienstleder M, Mertschnigg S, Schroettner H, Zankel A, Poteser M, Hutter H, Eppel Wand and Fitzek H, 2021 *Micron* **144** 103034
- [5] Jadavi S, Bianchini P, Cavalleri O, Dante S, Canale C and Diaspro A, 2021 *Microsc. Res. Tec.* **84** 2472-2482.
- [6] <https://www.zeiss.com/microscopy/en/resources/insights-hub/materials-sciences/sigma-rise-solution-for-multi-modal-correlative-microscopy.html>
- [7] Novotna V, Horak J, Konecny M, Hegrova V, Novotny O, Novacek Z and Neuman J, 2020 *Microscopy Today* **28** (3) 38-46
- [8] Dinarelli S, Mura F, Mancini C, La Penna G, Rinaldi T and Rossi M, 2022 *IOP Conf. Ser.: Mat. Sci. Eng.* **1265** 1 012011
- [9] Parlanti P and Cappello V, 2022 *Micron* **152** 103182
- [10] Echling P 2009 *Handbook of Sample Preparation for Scanning Electron Microscopy and X-ray Microanalysis* (Springer Science + Business Media, New York, USA)
- [11] <https://www.nenovision.com/>
- [12] <https://www.gwyddion.net/>
- [13] Goldstein J, Newbury DE, Joy DC, Lyman CE, Echlin P, Lifshin E, Sawyer L and Michael JR, 2003 *Scanning Electron Microscopy and X-Ray Microanalysis* (Kluwer Academic/Plenum Publishers, New York)